Journal of Hydrology 571 (2019) 605–618

Contents lists available at ScienceDirect

Journal of Hydrology

journal homepage: www.elsevier.com/locate/jhydrol

Research papers

Improving hydrological simulation in the Upper Mississippi River Basin through enhanced freeze-thaw cycle representation

Junyu Qi[a], Xuesong Zhang[a,b,*], Qianfeng Wang[c]

[a] Earth System Science Interdisciplinary Center, University of Maryland, College Park, 5825 University Research Ct, College Park, MD 20740, USA
[b] Joint Global Change Research Institute, Pacific Northwest National Laboratory and University of Maryland, College Park, MD 20740, USA
[c] College of Environment and Resources, Fuzhou University, Fuzhou, Fujian 350116, China

ARTICLE INFO

This manuscript was handled by Peter K. Kitanidis, Editor-in-Chief, with the assistance of Patrick Lachassagne, Associate Editor

Keywords:
Soil temperature
Freeze-thaw cycles
Streamflow
SWAT

ABSTRACT

Freeze-thaw cycles are important processes relevant to terrestrial hydrological cycling. However, the representation of freeze-thaw cycles has been often simplified in large scale watershed models. The Soil and Water Assessment Tool (SWAT), which has been widely used to understand and assess hydrologic budgets and water resources management, employs a simplified empirical approach to estimate soil temperature and determine the freezing and thawing status of soils. Here, we compared the performance of a physically-based soil temperature module and the built-in empirical approach in SWAT against field measurements at surface and 5, 10, 20, 50, and 100 cm depths at six stations of the U.S. Climate Reference Network (USCRN) within the Upper Mississippi River Basin (UMRB). In general, SWAT consistently underestimated winter soil temperatures and overestimated frozen days at all soil depths, while the modified version of SWAT (equipped with the physically-based soil temperature model; referred to as TSWAT) pronouncedly reduced the bias in estimated winter soil temperatures and frozen days compared with SWAT. Model performance assessment is conducted with three statistical coefficients, i.e., Bias (°C), the coefficient of determination (R^2), and Nash-Sutcliffe coefficient (NS). Statistical analyses show that TSWAT accurately simulated surface and soil temperatures at the five depths with R^2 and NS values greater than 0.82 at most sites, and Bias values were generally within the range of −1 to 1 °C during winter and ranged between −2.09 and 2.58 °C in non-winter seasons. The differences in freeze-thaw cycle representation between SWAT and TSWAT translate into noticeable discrepancies in simulated key hydrologic variables, such as surface runoff, percolation, and baseflow. Compared against long-term observed streamflow (1980–2015), TSWAT outperformed SWAT in capturing variations in monthly streamflow in both winter and non-winter seasons. These results and analyses highlight the value of improving freeze-thaw cycle representation for enhanced hydrologic modeling in large watersheds that are subject to freeze-thaw cycles.

1. Introduction

About 35% of the Earth's surface is subject to freeze-thaw cycles that have great hydrological and biogeochemical importance with respect to water security and climate change impacts (Li and Fang, 2016; Solomon, 2007; Williams and Smith, 1991). The presence of frozen soil layers significantly influences surface and subsurface exchanges of water and energy in the cold regions through hydrological and thermal processes (Ouyang et al., 2016; Wang et al., 2009; Woo et al., 2004). Freezing of soils reduces the hydraulic conductivity and results in more surface runoff due to decreased infiltration because of restricted drainage (Shanley and Chalmers, 1999; Slater et al., 1998). Phase changes of soil water are associated with latent heat absorption and release which have direct influences on the thermal regime of soils (Riseborough, 1990). Meanwhile, thermal gradients have considerable impacts on soil moisture migration (Cary, 1966). Energy exchange is particularly important in cold regions where freeze-thaw cycles have a critical influence on water infiltration and solute movement (Hayashi et al., 2003).

The coexistence of liquid water and ice in soils dramatically changes the thermal and hydraulic characteristics of the soil (Zhao et al., 1997). Ice content in soil layers directly controls infiltration and soil moisture movement (Cherkauer and Lettenmaier, 1999). Liquid water flow was unhindered at relative low ice content, while liquid water movement is restricted as the soil ice content increases (Harlan, 1973). In addition, the dynamics of soil heat fluxes are also depending on soil ice content

* Corresponding author at: Earth System Science Interdisciplinary Center, University of Maryland, College Park, 5825 University Research Ct, College Park, MD 20740, USA.
E-mail addresses: xzhang14@umd.edu, Xuesong.zhang@pnnl.gov (X. Zhang).

https://doi.org/10.1016/j.jhydrol.2019.02.020
Received 18 December 2018; Received in revised form 28 January 2019; Accepted 6 February 2019
Available online 16 February 2019

which determines the soil thermal properties (e.g., thermal conductivity and volumetric heat capacity) (Slater et al., 1998). The frozen depth in the soil profile is driven by the diurnal cycle of the soil surface temperature (Cherkauer and Lettenmaier, 1999). In general, the freezing front advances as the net heat flux out of the ground is positive, and a thawing front may form at the surface and advance into the soil as the net heat flux is negative (Cheng et al., 2014). The presence of snow cover further complicates the problem through its insulation effects which dampens daily heat fluxes and decreases frozen depth and timing (Groffman et al., 2001; Zhang, 2005). For example, an early snow that remains throughout the winter will result in shallower frozen depths than a late snow that falls after many days of cold weather (Iwata et al., 2011). Accurate simulation of the timing and depth of freeze-thaw boundary in hydrological models will significantly improve their ability to model the hydrologic processes in cold region (Luo et al., 2003; Woo et al., 2004). The inadequate representation of such freeze-thaw processes in most hydrology models is a crucial source of uncertainty in many hydrologic modeling studies. (Wellen et al., 2015; Zheng et al., 2018).

As a large-scale hydrological model, the Soil and Water Assessment Tool (SWAT) is designed to simulate hydrological processes and predict water quantity and quality as affected by landuse, management practices, and climate change at a watershed scale (Arnold et al., 1998). The SWAT model has been used worldwide to solve complex watershed management problems and modified for different study purposes (Gassman et al., 2007; Li et al., 2014; Qi et al., 2018a, 2017; Zhang et al., 2017). In SWAT, a watershed is partitioned into a number of subbasins, which are further discretized into hydrological response units (HRUs) based on specific combinations of landuse, soils, and slopes. The model calculates the water balance (i.e., surface and subsurface runoff, percolation and base flow, and evapotranspiration and transmission losses), crop growth, nutrient cycling, and pesticide movement at the HRU scale (Fontaine et al., 2002). Water flow, sediment, and nutrient loadings from each HRU in a subbasin are summed and the resulting loadings are then routed through channels, ponds, and reservoirs to the watershed outlet. In SWAT, soil temperature T_{soil} is calculated at the center of a soil layer (z) on the HRU scale by Neitsch et al. (2011),

$$T_{soil}(z) = \gamma \cdot T'_{soil}(z) + (1-\gamma)\cdot[d\cdot(\bar{T}_{Aair} - T_{sur}) + T_{sur}] \quad (1)$$

where γ is the lag coefficient that relates current day's temperature to that of the previous day, T'_{soil} is the soil temperature at a depth z on the previous day, d quantifies the influence of depth on soil temperature, $\bar{T}_{Aair}$ is the average annual air temperature, and T_{sur} is the temperature at soil surface. The depth factor d is a function of depth at the center of the soil layer (z), maximum damping depth, bulk density, and soil water. The soil surface temperature T_{sur} is determined by the previous day's temperature, the amount of ground cover, and the bare soil temperature which is a function of daily average, minimum, and maximum temperature as well as solar radiation reaching the ground and albedo. This empirical equation, in general, can reflect several features of temperature variation in soils: the annual soil temperature variation follows a sinusoidal function; the amplitude of the sine wave decreases with soil depth until temperature remains constant throughout the year at a certain depth; the timing of maximum and minimum temperatures varies with depth.

This empirical formulation works well in warm temperate regions. However, in cold regions with snow accumulation, predictions of soil temperature seldom agree with field measurements. For example, Bélanger (2009) pointed out, although the empirical formulation was able to simulate seasonal trends in soil temperature in the Canadian Boreal Plains, the formulation tended to underestimate soil temperature during winter, even with an adjusted lag coefficient. Snow has high surface albedo and emissivity and low thermal conductivity which can protect the ground from excessive heat loss in winter (Zhang, 2005). Although such effects have been partially accounted for in the SWAT model through the incorporation of correction factors (Neitsch et al., 2011), this does not fully address the physical processes driving soil temperature changes and, as a result, may not attend to the complexities associated with the presence of snow cover in winter (Bélanger, 2009). In addition, this empirical formulation does not simulate freeze-thaw cycles because phase changes of water are not considered in SWAT. As a result, hydrological processes influenced by freeze-thaw cycles cannot be accurately modeled at cold regions.

To overcome this problem, a physically-based soil temperature module has been developed in SWAT to consider the insulation effects of snow and latent heat exchange through phase changes of water in soils (Qi et al., 2016a,b). Instead of considering soil temperature as a function of air temperature, the new soil temperature module simulates temperature change in snow and soils as a result of heat conduction and latent heat exchange. Compared with the empirical soil temperature module, the new module can estimate snow or soil surface temperature based on an energy balance, update thermal properties of snow and soils according to changes in snow density and soil water/ice content, and simulate phase changes of water in the soil profile. The physically-based module was tested with field observed temperatures from a small experimental watershed in Atlantic Canada (Qi et al., 2016b), demonstrating an improvement in modeling soil temperatures. In the present study, we intend to achieve two objectives: (1) apply the modified version of SWAT (hereafter TSWAT) to a large-scale watershed, i.e., the Upper Mississippi River Basin (UMRB), to evaluate its capability of simulating freeze-thaw cycles across multiple sites; (2) compare TSWAT with the original SWAT model in simulating streamflow to understand the role of enhanced freeze-thaw cycle representation in a large scale watershed modeling.

2. Materials and methods

2.1. Study area

The UMRB extends from the source of the Mississippi River at Lake Itasca in northern Minnesota to a point just north of Cairo, Illinois with a total drainage area of 492,000 km^2 (Fig. 1) (Arnold et al., 2000). It constitutes a minor portion (15 percent) of the Mississippi River Basin system. Land cover in the basin includes agricultural lands, forest, wetlands, lakes, prairies, and urban areas. Nearly 69% of total land is used for agriculture and pasture with corn, soybeans, and alfalfa as the major crops in the basin (Wu and Tanaka, 2005). The UMRB contributes more than 50 percent of nitrogen transported to the Gulf of Mexico (Wu and Tanaka, 2005; Yuan et al., 2013) due to its intensive agricultural activities, landscape management, and widespread use of chemical fertilizers (Jha et al., 2004). The climate of the UMRB is subhumid continental with about 75% of the annual precipitation falls during corn growing season from April to October (Wu and Tanaka, 2005). Soil types in the basin range from heavy, poorly drained clay soil to light, well-drained sands.

2.2. Data collection

The SWAT model requires daily values of precipitation, max/min air temperature, solar radiation, relative humidity, and wind speed as forcing data. In the present study, we employed daily precipitation, max/min air temperature, solar radiation, relative humidity, and wind speed derived from the NASA North-American Land Data Assimilation System phase 2 (NLDAS; ldas.gsfc.nasa.gov/nldas/). NLDAS climate forcing data from 1979 to 2015 has assimilated multiple sources of climate observations and is widely recognized as a high resolution (~1/8°), spatially continuous, and comprehensive dataset that is valuable for water cycling studies (Xia et al., 2012). The spatial domain, spatial resolution, computational grid, terrain height, and land mask of NLDAS2 are identical to that in NLDAS1, which is described in Mitchell

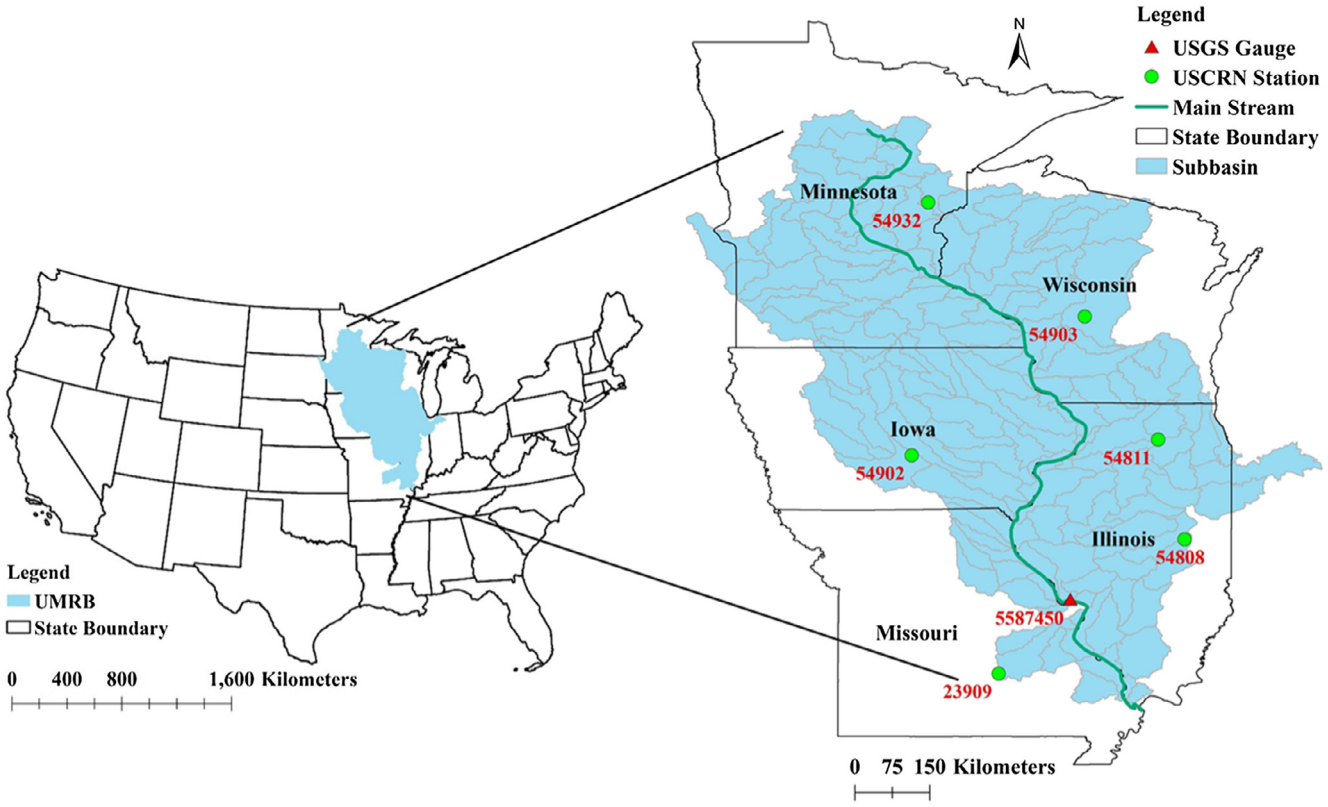

Fig. 1. Locations of Upper Mississippi River Basin (UMRB), six U.S. Climate Reference Network (USCRN) stations, and U.S. Geological Survey (USGS) gauge station # 05587450 within the basin.

et al. (2004).

Daily soil temperature records were derived from the U.S. Climate Reference Network (USCRN). USCRN is a systematic and sustained network of climate monitoring stations with sites across the conterminous U.S., Alaska, and Hawaii. In total, there are six USCRN stations evenly distributed in the UMRB (Fig. 1). USCRN stations are equipped with three soil probes measuring temperature and moisture at 5, 10, 20, 50, and 100 cm depths. In addition, each station measures ground surface temperature. USCRN stations are managed and maintained by the National Oceanic and Atmospheric Administration's (NOAA) National Centers for Environmental Information. The USCRN's primary goal is to provide long-term temperature, precipitation, and soil moisture and temperature observations that are of high quality and are taken in stable settings. The USCRN provides the United States with a reference network that meets the requirements of the Global Climate Observing System (GCOS). Monthly streamflow data were obtained for U.S. Geological Survey (USGS) gauge station # 05587450 (Grafton, Illinois) for the period of 1980–2015 (https://www.sciencebase.gov/catalog/item/5af49c2ae4b0da30c1b44e2b; Fig. 1).

2.3. Physically-based soil temperature module in SWAT

A physically-based soil temperature module has been developed and implemented in SWAT at the HRU scale based on heat transfer theory (Qi et al., 2016b),

$$\frac{\partial T}{\partial t} = \frac{\partial}{\partial x}\left(\frac{k}{C}\cdot\frac{\partial T}{\partial x}\right)\frac{s}{C} \quad (2)$$

where T is the temperature (°C), t represents the time step (in days), k is the thermal conductivity (J cm^{-1} d^{-1} °C^{-1}), C is the volumetric heat capacity (J cm^{-3} °C^{-1}), x is the vertical distance from the air-soil or air-snow interface (cm), and s is the latent heat source/sink term (J cm^{-3} d^{-1}). The calculated temperature was assumed to be uniform within individual layers as were the heat capacity and thermal conductivity which were functions of soil physical properties. The simulation domain was defined as extending from the air-soil or air-snow interface (upper boundary) to the damping depth (lower boundary), where the impact of air temperature diminishes (Fig. 2). When snow accumulated on the ground, the snow cover was treated as a single layer (Fig. 2).

2.3.1. Boundary conditions

The upper boundary temperature was determined by the energy balance equation (Hillel, 1980),

$$R_{sn} + R_{ln} + LE + H + S = 0 \quad (3)$$

where R_{sn} is the net solar radiation, R_{ln} is the net longwave radiation, LE is the latent heat flux, H is the sensible heat flux, and S is the ground conductive heat transfer. All energy terms in Eq. (3) have the same unit: J cm^{-2} d^{-1}. Latent and sensible heat were determined as in Meng et al. (1995) and Yin and Arp (1993),

$$LE + H = h_e\cdot(T_a - T_0) \quad (4)$$

where T_a is the air temperature (°C), T_0 is the surface temperature (°C), and h_e is the effective surface heat transfer coefficient (J cm^{-1} d^{-2} °C^{-1}). h_e is defined as a lumping coefficient that characterized the air-surface heat transfer rate and the heat transfer rate associated with the shading and insulative properties of the overlying vegetation and residue. The ground conductive heat flux was defined as,

$$S = \frac{k_1}{0.5\cdot x_1}\cdot(T_0 - T_1) \quad (5)$$

where k_1 is the thermal conductivity of the top layer (J cm^{-1} d^{-1} °C^{-1}), x_1 is the thickness of the top layer (cm), T_1 is the temperature at the center of the top layer (°C). In the absence of snow cover, the first soil layer was referred to the top layer.

Based on Eqs. (3)–(5), the surface temperature was determined by,

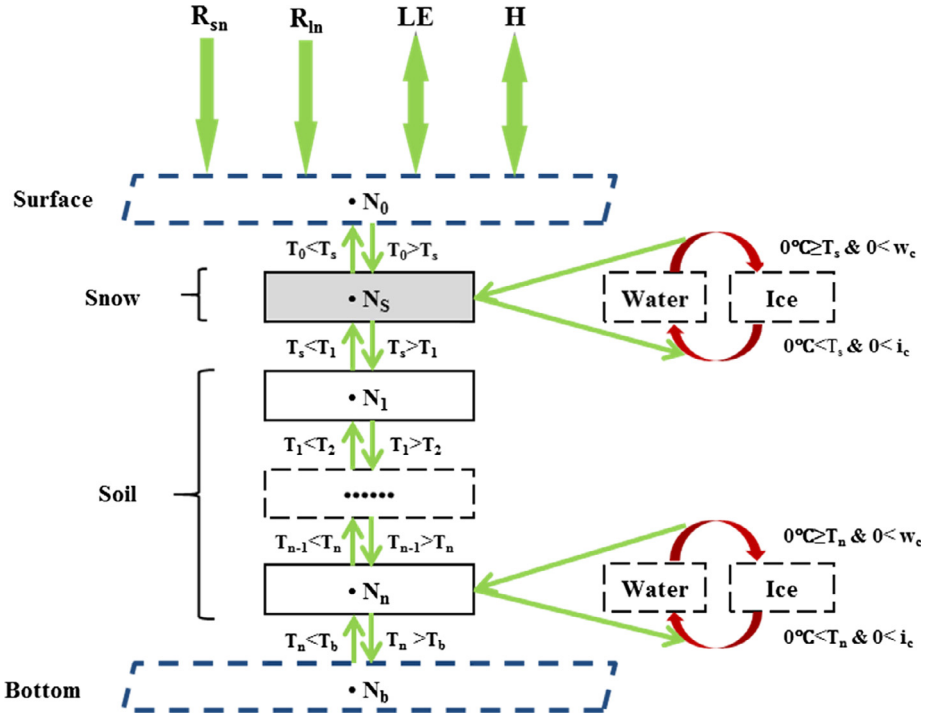

Fig. 2. Schematic flowchart of heat conduction in snow and soil layers. The freeze-thaw processes with latent heat release and absorption are also illustrated. R_{sn} is the net solar radiation, R_{ln} is the net longwave radiation, LE is the latent heat flux, H is the sensible heat flux, T_n is the temperature for *nth* node (N_0 and N_b are the surface and bottom nodes; N_s is the node at the center of the snow layer; N_1 to N_n are nodes centered at each soil layer), and i_c and w_c are ice and water content in each soil layer. Green arrows indicate heat transfer processes and red arrows indicate mass transfer processes. (For interpretation of the references to color in this figure legend, the reader is referred to the web version of this article.)

Table 1
Location of identified six USCRN stations in the UMRB and their soil types and data ranges used in SWAT simulation.

Site name	Station no.	Lon.	Lat.	Soil texture	Data used
Audubon Center of the North Woods	54,932 (MN)	−93.29	41.56	Silt Loam	2011–2015
Necedah National Wildlife Refuge	54,903 (WI)	−88.37	40.05	Silt Loam	2009–2015
Northern Illinois Agronomy Research Center	54,811 (IL)	−88.85	41.84	Silt Loam	2009–2015
Neal Smith National Wildlife Refuge	54,902 (IA)	−92.99	46.11	Clay Loam	2009–2015
White River Trace Conservation Area	23,909 (MO)	−91.72	37.63	Silt Loam	2009–2015
Bondville Environmental & Atmospheric Research Station	54,808 (IL)	−90.17	44.06	Loamy Sands	2009–2015

Table 2
Calibrated parameter values for the soil temperature module for the six USCRN stations.

Station	Parameter	Used value	Station	Parameter	Used value
MN54932	eff_{coe}	64.03	WI54903	eff_{coe}	68.45
	k_{coe}	17.36		k_{coe}	8.96
	k_{s_coe}	3.92		k_{s_coe}	4.99
	c_{coe}	14.12		c_{coe}	17.81
IL54811	eff_{coe}	29.48	IA54902	eff_{coe}	51.15
	k_{coe}	7.87		k_{coe}	7.53
	k_{s_coe}	8.00		k_{s_coe}	11.00
	c_{coe}	9.36		c_{coe}	13.76
MO23909	eff_{coe}	60.88	IL54808	eff_{coe}	58.10
	k_{coe}	18.25		k_{coe}	8.23
	k_{s_coe}	14.03		k_{s_coe}	17.08
	c_{coe}	5.73		c_{coe}	13.64

Note: k_{coe} and k_{s_coe} is used to calibrate soil and snow thermal conductivities; c_{coe} is used to calibrated heat capacity of soil layers; eff_{coe} is the effective air-to-ground conductance ratio.

$$T_0 = \frac{T_a}{1+\beta_e} + \frac{\beta_e}{1+\beta_e}\cdot\left[T_1 + \frac{R_{ln}+R_{sn}}{2\cdot k_1/x_1}\right] \quad (6)$$

where parameter $\beta_e = \frac{k_1/(x_1/2)}{h_e}$, which is the effective air-to-ground conductance ratio (dimensionless), which denotes the relative rate between surface-soil heat transfer and air-surface heat transfer. Low β_e indicates that the rate of heat conductance into the soil profile through the top layer is low (k_1 approaches 0), or the rate of air-to-surface heat exchange is high (greater h_e values). With greater h_e values, the surface temperature tends to quickly equilibrate to air temperature (i.e., T_0 converges to T_a). Parameter β_e was calibrated with an empirical equation (Eq. (7)) developed by Yin and Arp (1993).

$$\beta_e = eff_{coe}\cdot R_{sn}\cdot\left(1 - e^{\min(V_c,V_v)-6.8}\right) \quad (7)$$

We found that β_e closely correlates with net solar radiation R_{sn} and vegetative area indexes (V_c and V_v). Parameter eff_{coe} is a coefficient to calibrate β_e, and the default value of eff_{coe} is 8.1 according to Yin and Arp (1993) for forest lands. For agricultural lands, eff_{coe} is close to 50 according to previous studies (Qi et al., 2016a,b).

The amount of net solar radiation and net longwave radiation was calculated using the algorithms in SWAT (Neitsch et al., 2011). The lower boundary of the simulation domain was defined at the damping depth determined by SWAT. Soil temperature T_z (°C) at this depth was determined following the method in Steppuhn (1981).

2.3.2. Soil and snow thermal properties

Johansen (1975) developed a method to determine soil thermal conductivity for unfrozen and frozen soils. The thermal conductivity of unsaturated soils (k) was determined by its thermal conductivities in dry (k_{dry}) and saturated (k_{sat}) states, by introducing a Kersten number, i.e., K_e. The K_e was determined by the degree of saturation, which was calculated from the amount of water or ice in the soil. For saturated soils, a geometric mean equation based on the thermal conductivities of the components and their respective volumetric fractions was used in the calculation of thermal conductivity. Parameter k_{coe} was used to

Table 3
Statistical assessment of model performance for simulating daily surface and soil temperatures at different depths for the six USCRN stations during their periods of record.

			TSWAT				SWAT			
Depth	Station	Obs-Mean (℃)	R^2	NS	Mean (℃)	Bias (℃)	R^2	NS	Mean (℃)	Bias (℃)
Surface	MN54932	5.61	0.91	0.90	7.01	1.4				
	WI54903	9.28	0.90	0.89	8.37	-0.91				
	IL54811	9.72	0.92	0.91	10.48	0.76				
	IA54902	10.08	0.90	0.89	11.15	1.07				
	MO23909	12.74	0.85	0.82	14.42	1.68				
	IL54808	10.49	0.86	0.80	13.28	2.79				
5cm	MN54932	7.71	0.95	0.89	8.74	1.03	0.89	0.60	7.02	-0.69
	WI54903	10.34	0.95	0.95	9.66	-0.68	0.94	0.86	7.54	-2.80
	IL54811	10.73	0.97	0.95	10.77	0.04	0.96	0.92	10.27	-0.46
	IA54902	10.76	0.97	0.92	12.06	1.30	0.95	0.90	11.27	0.51
	MO23909	13.62	0.96	0.92	14.76	1.14	0.95	0.92	14.41	0.79
	IL54808	11.83	0.96	0.92	13.35	1.52	0.96	0.93	13.02	1.19
10cm	MN54932	7.87	0.95	0.90	8.69	0.82	0.88	0.62	6.93	-0.94
	WI54903	10.17	0.95	0.95	9.62	-0.55	0.94	0.86	7.28	-2.89
	IL54811	10.63	0.97	0.95	10.65	0.02	0.96	0.93	10.11	-0.52
	IA54902	10.77	0.97	0.92	12.02	1.25	0.95	0.90	11.15	0.38
	MO23909	13.72	0.96	0.93	14.75	1.03	0.95	0.93	14.19	0.47
	IL54808	11.89	0.96	0.92	13.31	1.42	0.96	0.94	12.91	1.02
20cm	MN54932	7.7	0.95	0.90	8.61	0.91	0.86	0.63	6.77	-0.93
	WI54903	10.28	0.95	0.95	9.55	-0.73	0.93	0.81	6.91	-3.37
	IL54811	10.79	0.97	0.95	10.66	-0.13	0.95	0.93	10.05	-0.74
	IA54902	10.98	0.97	0.94	11.96	0.98	0.93	0.90	10.92	-0.06
	MO23909	13.78	0.97	0.93	14.73	0.95	0.93	0.93	13.81	0.03
	IL54808	11.83	0.96	0.92	13.26	1.43	0.95	0.94	12.74	0.91
50cm	MN54932	7.69	0.95	0.92	8.51	0.82	0.83	0.72	6.33	-1.36
	WI54903	10.15	0.92	0.89	9.4	-0.75	0.87	0.64	6.27	-3.88
	IL54811	11.14	0.96	0.95	10.58	-0.56	0.89	0.86	9.72	-1.42
	IA54902	11.15	0.96	0.95	11.9	0.75	0.86	0.85	10.58	-0.57
	MO23909	13.78	0.98	0.93	14.72	0.94	0.83	0.82	13.22	-0.56
	IL54808	11.95	0.95	0.92	13.2	1.25	0.89	0.88	12.39	0.44
100cm	MN54932	7.82	0.93	0.92	8.35	0.53	0.73	0.61	5.67	-2.15
	WI54903	10.23	0.65	0.60	9.26	-0.97	0.74	0.28	6.06	-4.17
	IL54811	11.29	0.91	0.85	10.47	-0.82	0.71	0.59	9.28	-2.01
	IA54902	11.31	0.90	0.89	11.85	0.54	0.66	0.59	10.18	-1.13
	MO23909	13.8	0.98	0.95	14.75	0.95	0.75	0.61	12.97	-0.83
	IL54808	11.9	0.89	0.84	13.17	1.27	0.68	0.66	12.06	0.16

Note: Shaded numbers indicate SWAT has a lower absolute value of Bias or higher values of NS or R^2 than the corresponding values for TSWAT.

calibrate soil thermal conductivities,

$$k = k_{coe}\cdot[(k_{sat} - k_{dry})\cdot K_e + k_{dry}] \quad (8)$$

The volumetric heat capacity of soils (C_{soil}; J cm^{-3} °C^{-1}) was calculated as the volumetric weighted mean of the specific heat capacity of soil constituents and calibrated by a parameter c_{coe} as a multiplier, i.e.,

$$C_{soil} = c_{coe}\cdot(C_m\cdot m_c + C_o\cdot o_c + C_w\cdot w_c + C_i\cdot i_c) \quad (9)$$

where C_m, C_o, C_w, and C_i are volumetric heat capacity of soil minerals, organic matter, water and ice (J cm^{-3} °C^{-1}), and m_c, o_c, w_c, and i_c are corresponding volumetric contents. The volumetric heat capacity of the air in soil void space is negligible compared with other constituents.

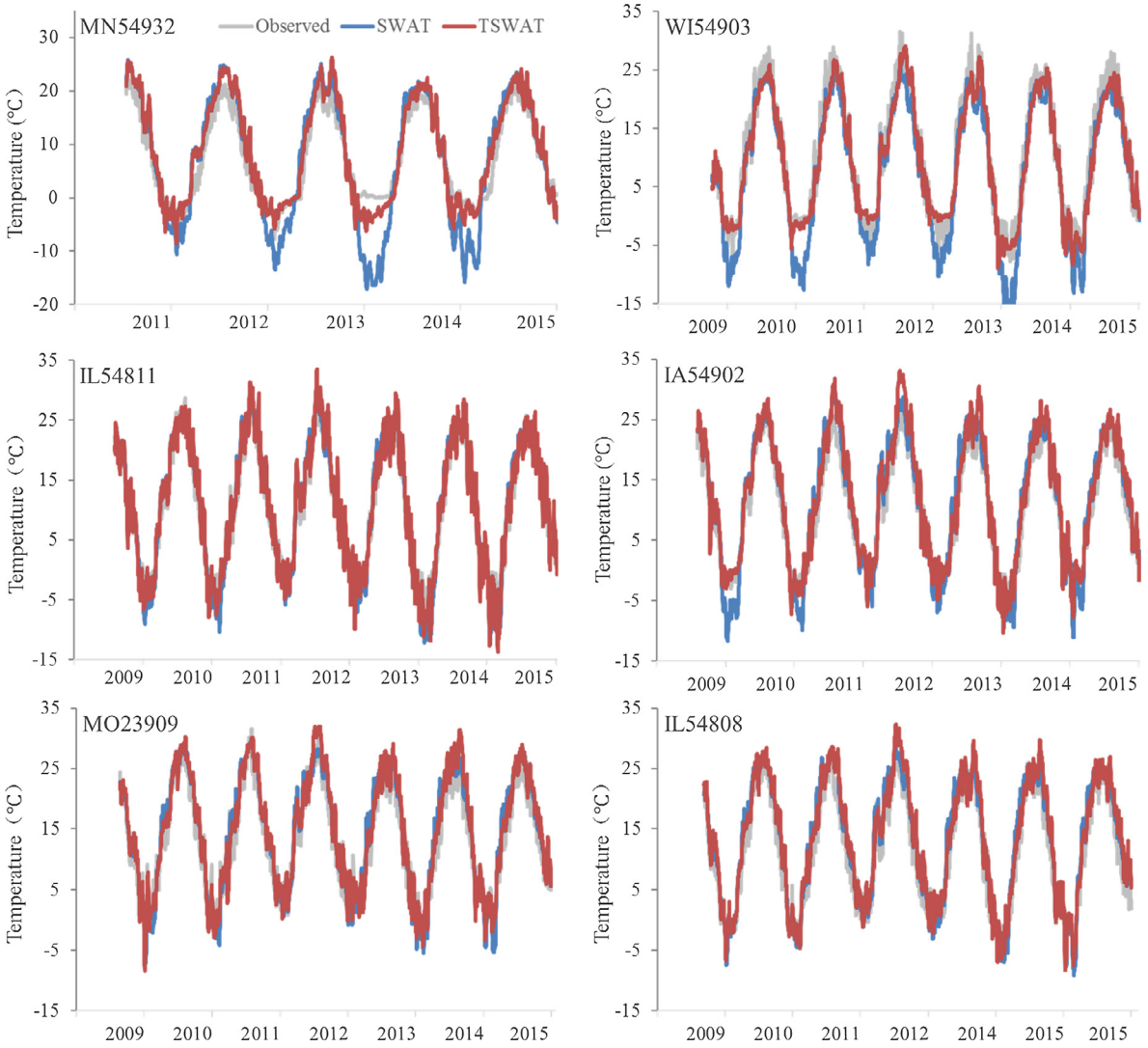

Fig. 3. Simulated vs. observed daily soil temperature at 5 cm depth for the six USCRN stations.

The thermal conductivity of snow was calculated as a function of snow density according to Sturm et al. (1997). Snow density was linearly correlated to snow water equivalent *SNO* (Jonas et al., 2009). The snow depth was a function of snow density and *SNO*. The *SNO* was calculated with the snow module of SWAT. Parameter k_{s_coe} calibrated the thermal conductivity of the snow layer as a multiplier. The volumetric heat capacity of snow was calculated based on Verseghy (1991).

2.3.3. Latent heat exchange

The new soil-temperature module considered latent heat transfer due to freeze-thaw cycles as an internal heat source or sink within individual soil layers (Fig. 2). Latent heat was calculated according to the release of energy during the freezing of liquid water and the absorption of energy during the melting of ice (Fig. 2). Each layer froze when its temperature reached or fell below 0 °C and thawed when its temperature exceeded 0 °C (Fig. 2). Volumetric soil ice and water content were updated at the daily time step based on the status of the soil with respect to freezing or thawing (Fig. 2). Detailed information regarding module development including above-mentioned functions and variables could be found in Qi et al. (2016b).

2.4. SWAT model setup and soil temperature calibration

The SWAT model requires a variety of detailed information describing the land use, soil, and topography data of the UMRB. The present study adopted a previously established UMRB SWAT project but running with latest version of SWAT (ver. 664). In the previous study, the UMRB was divided into 131 subbasins according to the eight-digit United States Geological Survey (USGS) hydrologic unit codes (HUCs; Fig. 1). National Hydrography Dataset (NHD) stream dataset and a 90 m digital elevation model (DEM) was used to provide watershed configuration and topographic parameter estimation. A land use map was created by combing two sources of information, i.e., the Cropland Data Layer (CDL) and 2001 National Land Cover Data to better define cultivated and non-agricultural land use. The State Soil Geographic (STATSGO) database 1:250,000 scale soil map was used for UMRB. Using a threshold operation of 5% for land use, 10% for soil, and 5% for slope, 14,568 HRUs were generated and the number of HRUs per subbasin ranged from 58 to 216. Management practices such as tile drainage, tillage, crop rotation, and fertilizer and manure application were included in the project according to various sources. Detailed model setup information can be found in Srinivasan et al. (2010).

The six soil temperature monitoring stations were identified at the corresponding HRUs in the UMRB using ArcGIS (Fig. 1). Corresponding soil types and slope classes are shown in Table 1. The TSWAT model was used to simulate soil temperatures at 5, 10, 20, 50, and 100 cm depths in the six identified HRUs with Particle Swarm Optimization (PSO) algorithm of SWAT-CUP to calibrate four relevant parameters

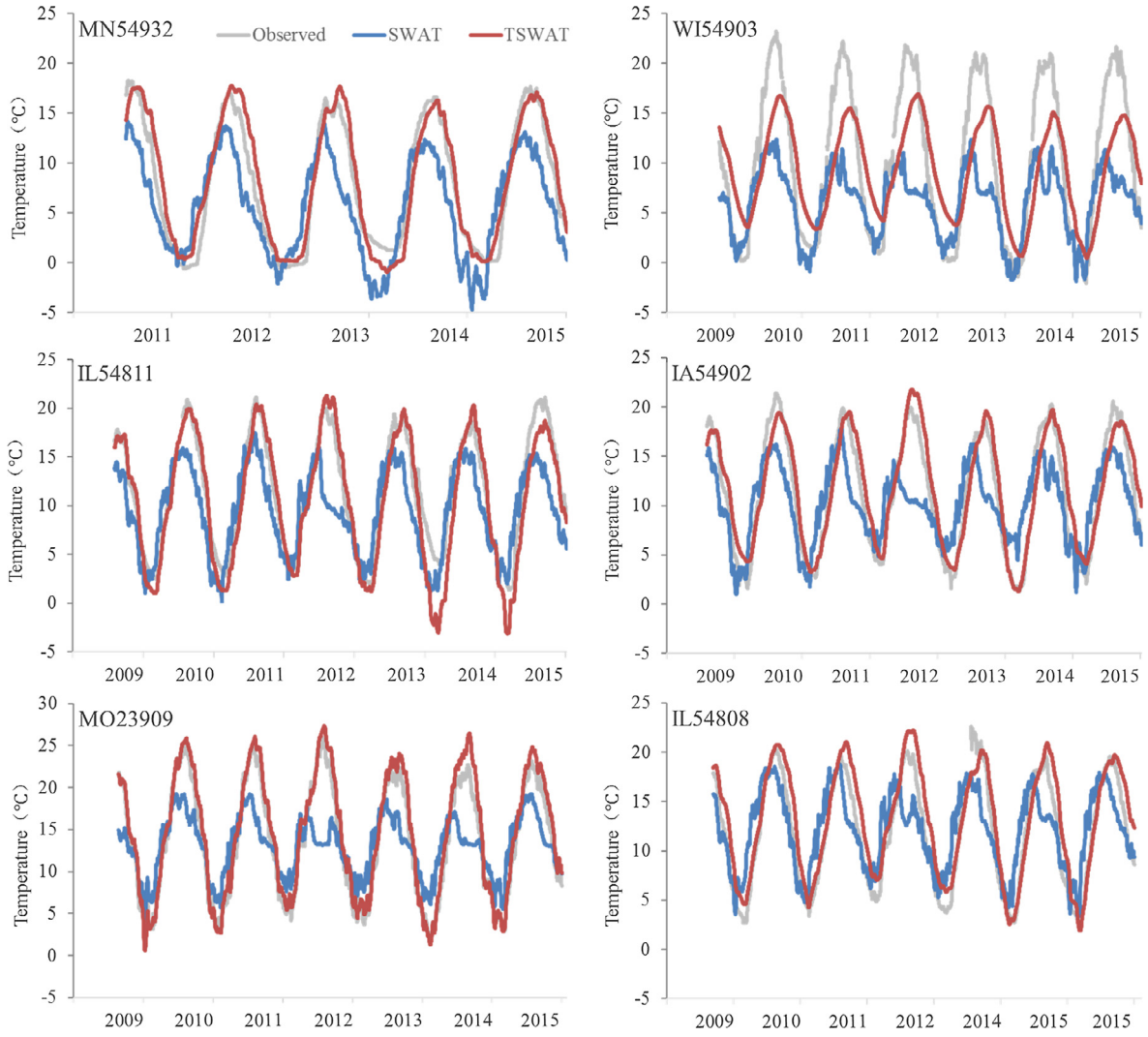

Fig. 4. Simulated vs. observed daily soil temperature at 100 cm depth for the six USCRN stations.

(i.e., eff_{coe}, k_{coe}, k_{s_coe}, and c_{coe}). Specifically, the PAO algorithm was applied to each site with hundreds of simulations by each iteration (iteration and simulation numbers varies at different sites). In order to simulate hydrology at the watershed scale, we applied the optimized parameters of the six HRUs to other HRUs in the basin using the nearest neighbor method via ArcGIS. The surface temperature records from the six stations were used to validate the model.

2.5. Model evaluation

Model performance was assessed according to three coefficients of accuracy, i.e., Bias (°C), the coefficient of determination (R^2), and Nash-Sutcliffe coefficient (NS) as described by Moriasi et al. (2007):

$$\text{Bias} = O_{avg} - P_{avg} \tag{10}$$

$$NS = 1 - \frac{\sum_{i=1}^{n}(O_i - P_i)^2}{\sum_{i=1}^{n}(O_i - O_{avg})^2} \tag{11}$$

$$R^2 = \left(\frac{\sum_{i=1}^{n}(O_i - O_{avg})\cdot(P_i - P_{avg})}{[\sum_{i=1}^{n}(O_i - O_{avg})^2 \cdot \sum_{i=1}^{n}(P_i - P_{avg})^2]^{0.5}} \right)^2 \tag{12}$$

where O_i and P_i are the observed and predicted values, O_{avg} and P_{avg} are the average of the observed and predicted values. Model performance on stream flow at the USGS gauge station # 05587450 was assessed by R^2, NS and percent bias, i.e.,

$$P_{bias} = 100 \cdot \frac{(O_{avg} - P_{avg})}{O_{avg}} \tag{13}$$

3. Results and discussion

3.1. Soil temperature model calibration

Table 2 shows the calibrated parameter values for the physically-based soil temperature module at the six USCRN stations. The values of parameter eff_{coe} (calibrating surface energy) ranged from 29.48 to 68.45 (with most values ranging from 51.15 to 68.45) and the values of parameter k_{coe} (calibrating soil thermal conductivity) ranged from 7.53 to 18.25. These results are generally consistent with the values (i.e., eff_{coe} = 50 and k_{coe} = 10) determined in previous studies conducted in cold climates (Qi et al., 2016a,b). In the present study, we also calibrated the parameter k_{s_coe} (for snow thermal conductivity) and c_{coe} (for soil heat capacity) which were not calibrated in the previous studies (i.e., default values = 1 was used for both parameters). The values of parameter k_{s_coe} ranged from 3.92 to 17.08 while the values of parameter c_{coe} ranged from 5.73 to 17.81. The reason for increased thermal conductivity for soil layers in the previous studies and also in the present studies is because SWAT tended to underestimate soil moisture which has much higher thermal conductivity compared with void soil

Table 4
Simulated vs. observed mean daily surface and soil temperatures (°C) at different depths and corresponding biases at the six USCRN stations for winter (Nov. to Apr.) and non-winter seasons.

			Winter						Non-Winter					
Station			Surface	5cm	10cm	20cm	50cm	100cm	Surface	5cm	10cm	20cm	50cm	100cm
MN54932		Observed (°C)	-4.56	0.08	0.35	0.51	1.01	2.03	15.00	13.85	13.91	13.47	13.05	12.48
	TSWAT	Simulated (°C)	-3.61	-0.25	-0.01	0.40	1.34	2.73	16.24	15.97	15.68	15.21	14.27	12.86
		Bias (°C)	0.95	-0.33	-0.36	-0.11	0.33	0.70	1.24	2.12	1.77	1.73	1.21	0.38
	SWAT	Simulated (°C)		-4.14	-16.11	-3.09	-1.37	-1.12		15.99	15.53	14.69	12.52	9.32
		Bias (°C)		-4.22	-16.46	-3.60	-2.38	-3.15		2.14	1.62	1.22	-0.53	-3.16
WI54903		Observed (°C)	-1.13	1.44	1.40	1.78	2.34	3.46	19.30	18.62	18.33	18.20	17.42	16.52
	TSWAT	Simulated (°C)	-1.71	1.04	1.18	1.57	3.03	5.96	17.87	17.71	17.51	17.00	15.33	12.30
		Bias (°C)	-0.59	-0.40	-0.22	-0.21	0.68	2.51	-1.43	-0.91	-0.83	-1.20	-2.09	-4.22
	SWAT	Simulated (°C)		-2.22	-1.83	-1.10	0.77	3.30		16.63	15.76	14.36	11.39	8.64
		Bias (°C)		-3.66	-3.23	-2.88	-1.57	-0.16		-1.99	-2.57	-3.84	-6.03	-7.88
IL54811		Observed (°C)	0.18	2.44	2.59	3.03	4.14	6.17	17.80	18.13	17.88	17.71	17.38	15.94
	TSWAT	Simulated (°C)	1.14	1.67	1.80	2.12	3.23	4.96	19.21	18.99	18.77	18.35	17.20	15.56
		Bias (°C)	0.96	-0.77	-0.78	-0.91	-0.91	-1.21	1.41	0.86	0.89	0.64	-0.18	-0.38
	SWAT	Simulated (°C)		0.82	1.17	1.82	3.53	5.64		18.70	18.23	17.39	15.25	12.66
		Bias (°C)		-1.62	-1.42	-1.21	-0.61	-0.53		0.57	0.35	-0.32	-2.13	-3.28
IA54902		Observed (°C)	0.78	2.76	3.02	3.52	4.29	5.98	18.39	17.74	17.52	17.48	17.14	15.97
	TSWAT	Simulated (°C)	1.55	3.06	3.27	3.71	5.18	7.33	20.10	19.89	19.63	19.13	17.73	15.72
		Bias (°C)	0.77	0.30	0.25	0.20	0.89	1.35	1.72	2.15	2.11	1.64	0.59	-0.25
	SWAT	Simulated (°C)		1.88	2.29	3.07	4.86	7.11		19.45	18.87	17.78	15.56	12.87
		Bias (°C)		-0.88	-0.73	-0.45	0.57	1.13		1.71	1.35	0.30	-1.58	-3.10
MO23909		Observed (°C)	4.97	6.33	6.52	6.88	7.39	7.70	19.49	20.03	20.05	19.84	19.39	19.16
	TSWAT	Simulated (°C)	6.24	6.61	6.71	6.90	7.43	8.18	22.07	21.94	21.83	21.62	21.15	20.53
		Bias (°C)	1.27	0.28	0.19	0.03	0.04	0.49	2.58	1.91	1.78	1.78	1.76	1.37
	SWAT	Simulated (°C)		6.15	6.44	7.01	8.51	10.30		21.67	20.99	19.78	17.35	15.32
		Bias (°C)		-0.18	-0.08	0.13	1.12	2.60		1.64	0.94	-0.06	-2.04	-3.84
IL54808		Observed (°C)	1.50	3.89	4.17	4.46	5.46	6.90	18.06	18.94	18.80	18.44	17.76	16.40
	TSWAT	Simulated (°C)	4.63	4.87	5.07	5.49	6.80	8.74	21.23	20.97	20.71	20.23	18.93	17.14
		Bias (°C)	3.14	0.98	0.90	1.03	1.34	1.84	3.16	2.03	1.91	1.79	1.17	0.74
	SWAT	Simulated (°C)		4.46	4.77	5.34	6.88	8.81		20.69	20.21	19.38	17.34	14.99
		Bias (°C)		0.57	0.60	0.88	1.42	1.91		1.75	1.41	0.94	-0.42	-1.41

Note: Shaded numbers indicate SWAT has lower absolute values of Bias than the corresponding values of TSWAT.

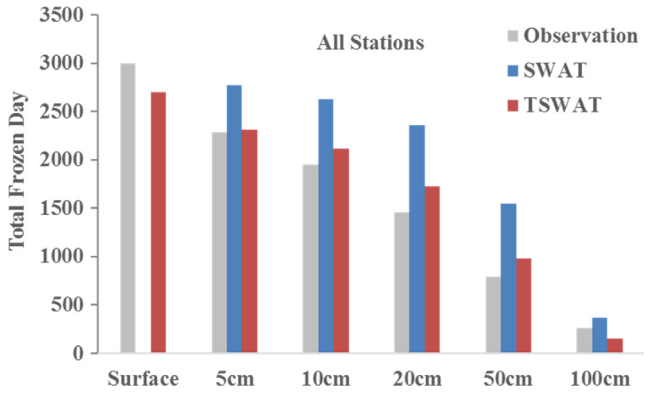

Fig. 5. Total number of simulated vs. observed frozen days (temperature ≤0 °C) for surface and soil layers at different depths summarized over the six USCRN stations during their periods of record (see Table 1) by two versions of SWAT model.

air space (Qi et al., 2018b). The larger-than-default values of c_{coe} can partially compensate overestimated thermal conductivity due to unevenly distributed soil moisture in the entire soil profile. k_{s_coe} was calibrated to better address snow insulation effects on soil temperature.

3.2. Model performance evaluation for soil temperature

Model performance of TSWAT on daily temperatures at surface and five different soil depths in the six USCRN stations was evaluated based on R^2, NS, and Bias (Table 3). Model performance of the original version of SWAT model (with the empirical soil temperature module) at five soil depths were also illustrated in Table 3 (daily surface temperature is not simulated by the original SWAT model). Simulated and observed mean daily temperatures for periods of record for each station (see Table 1) are also included. In general, TSWAT accurately simulated surface and soil temperatures with higher accuracy for top soil layers than for deeper soil layers. The R^2 and NS values are greater than 0.82 except for station WI54903 at 100 cm depth (Table 3). Based on Bias values, TSWAT slightly overestimated surface and soil temperatures at different soil depths except for stations WI54903 and IL54811 (Table 3). All R^2 values of TSWAT were greater than the corresponding values of SWAT at different soil depths for different stations. Most NS values of TSWAT were also greater than those of SWAT except for station IL54808 at soil depths of 5, 10, 20 cm (Table 3). The absolute Bias values of TSWAT were generally less than the corresponding values of SWAT for stations in the northern portion of the basin at different soil depths (Table 3; Fig. 1). This indicates that the physically-based soil temperature module outperformed the empirical soil temperature module especially in areas with seasonal snow cover. On the other hand, the empirical soil temperature model was able to capture the average conditions of soil temperatures especially at top soil layers in a temperate climate.

To illustrate the contrasting performance of TSWAT and SWAT for top and deep soil layers, we show simulated vs. observed daily soil temperature time series at 5 and 100 cm depths in Figs. 3 and 4, respectively. TSWAT performed better than SWAT at describing the variations of daily soil temperature in winter at the top soil layer and for the whole year at the deepest soil layer. In fact, SWAT severely underestimated winter soil temperatures at the top soil layers while TSWAT was able to simulate winter soil temperatures more accurately which was the precondition of simulating freeze-thaw cycles in winter. At deeper soil layers, although SWAT could capture the general trend of seasonal variations in soil temperature, it had large biases with respect

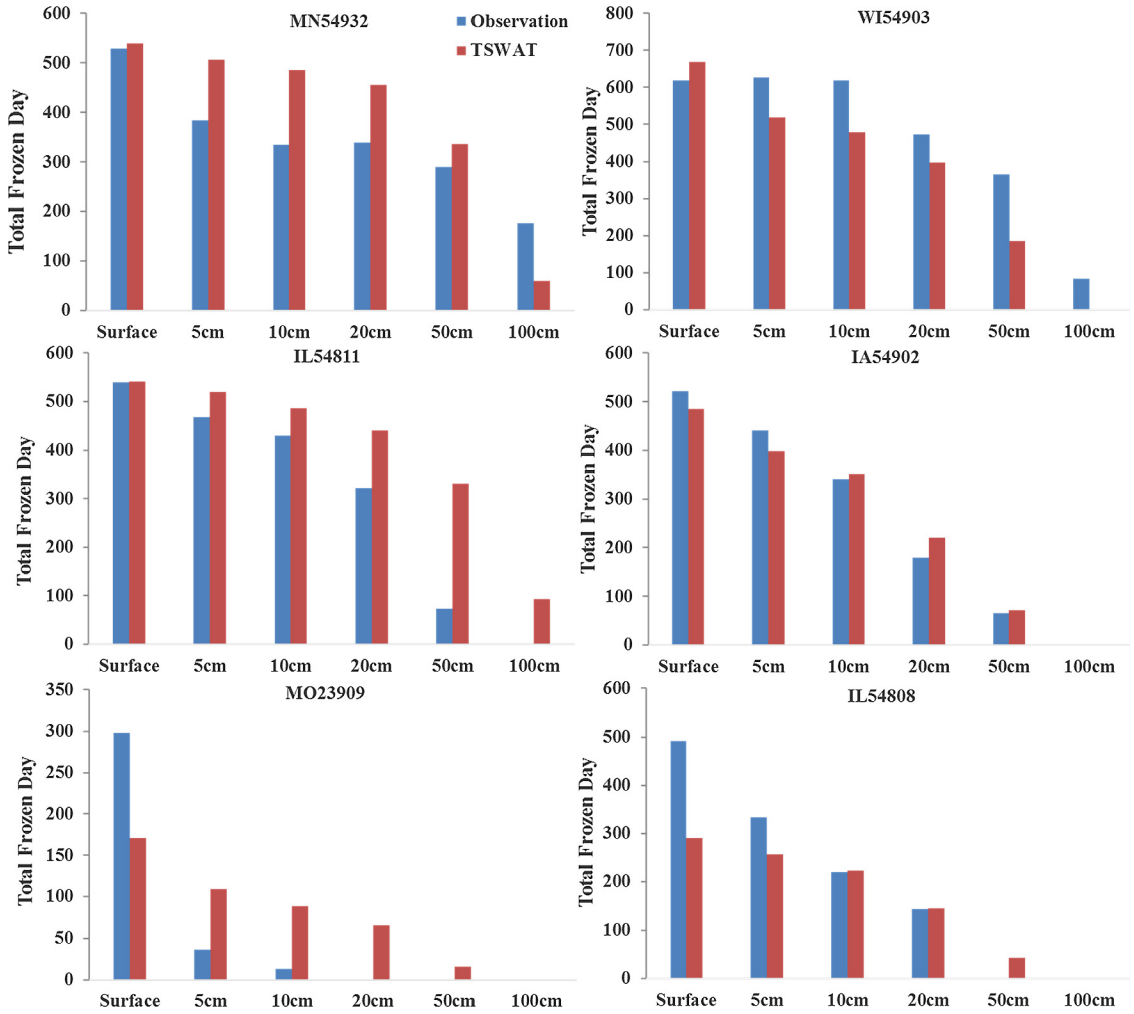

Fig. 6. Total number of simulated vs. observed frozen days (temperature ≤0 °C) for surface and soil layers at different depths for the six USCRN stations during their periods of record (see Table 1) by the TSWAT model.

to summer temperature peaks (Fig. 4). The poorer performance for both versions of SWAT at the 100 cm depth for station WI54903 may be caused by uncertainties associated with soil physical properties at deeper soil layers.

We also added analyses with respect to winter and non-winter seasons to evaluate model performance based on Bias at the surface and five different soil depths for the six USCRN stations as shown in Table 4. For TSWAT, most Bias values (°C) were within the range of −1 to 1 °C during winter for different stations. This is especially true for the surface and top soil layers (i.e., soil depths < 100 cm; Table 4). Even for soil layer at 100 cm depth, the Bias values were within the range of −1.21 to 2.51 °C. For non-winter seasons, however, the TSWAT model tended to have slightly greater absolute values of Bias. The maximum Bias value was 3.16 °C at the surface of IL54808, while the minimum value was −4.22 °C at 100 cm depth of WI54903. Except for these two extremes, the Bias values ranged from −2.09 to 2.58 °C for other data points (Table 4). The model tended to overestimate surface and soil temperatures during non-winter seasons while this was not obvious during winter (Table 4).

In most stations, absolute values of Bias for SWAT were greater than the corresponding values of TSWAT, and the discrepancies between the absolute values of Bias for SWAT and TSWAT were greatest at top soil layers and then decreased with soil depth in winter (Table 4). Note that the Bias values of soil temperature at 10 cm depth was −16.46 and −0.36 °C for SWAT and TSWAT, respectively, in station MN54932 (with the highest latitude; Fig. 1) which demonstrated again that the empirical soil temperature module severely underestimated winter soil temperatures in top soil layers. On the contrary, absolute values of Bias for SWAT were slightly less than the corresponding values of TSWAT at top soil layers for most stations while TSWAT tended to have lower absolute values of Bias at deeper soil layers in all stations in the non-winter seasons (Table 4). These results explained the reason for lower absolute values of Bias of SWAT than those of TSWAT in stations in the southern portion of the basin on the annual temporal scale in Table 3. As a result, the physically-based soil temperature model pronouncedly improved winter soil temperature simulation which is the basis for accurate simulate soil freeze-thaw cycles.

3.3. Model performance evaluation for estimated frozen days

To clarify small biases that may accumulate over time, we calculated the total number of frozen days (with temperature ≤ 0 °C) as observed and simulated by SWAT and TSWAT for each soil layer over all sites and their periods of record (Fig. 5). Note that the original SWAT model does not simulate soil surface temperature. We used percent bias (P_{bias} in %; Eq. (13)) to evaluate model performance. For TSWAT, the highest accuracy was found at 5 cm depth with P_{bias} of −1% and the lowest accuracy was at 100 cm depth with P_{bias} of 41%. For the surface and other soil depths, P_{bias} ranged from −24 to 10%. In general, simulated frozen days were less than observed for the surface and 100 cm soil depth while more than observed for soil depths from 5 to 50 cm (Fig. 5). For the original SWAT model, the highest accuracy was also

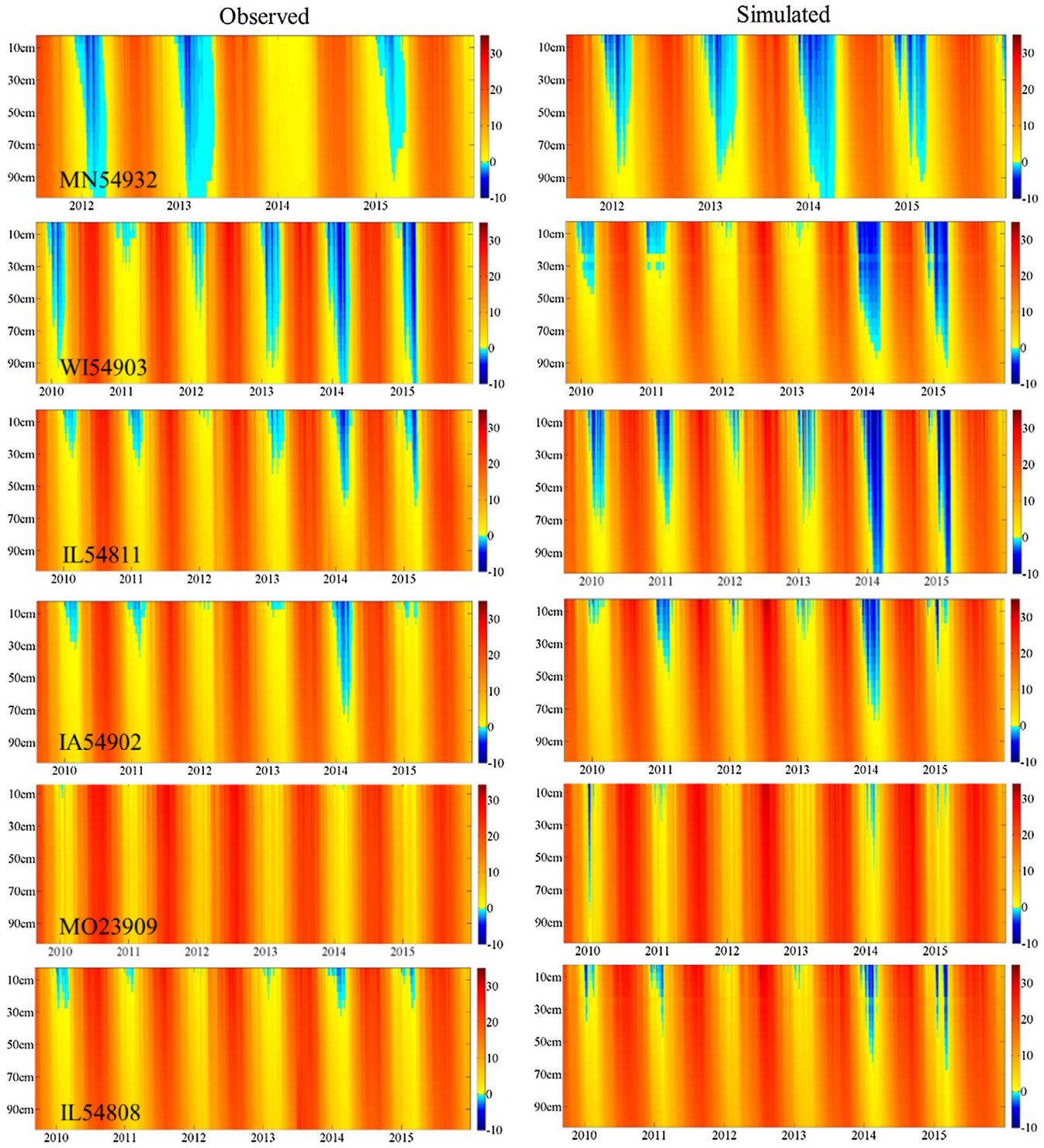

Fig. 7. Simulated vs. observed soil profile temperature (temperature ≤ 0 °C) for the six USCRN stations by TSWAT. The color ramp on the right of each figure shows the temperature represented in different colors, with bluish colors indicating frozen status and reddish colors indicating temperatures above 0 °C.

found at 5 cm soil depth but with a much lower P_{bias} of −21% and the lowest accuracy was at 50 cm depth with P_{bias} of −96%. P_{bias} values ranged from −34 to −62% at other soil depths. In general, SWAT pronouncedly overestimated frozen days than TSWAT mainly because the empirical soil temperature module tended to underestimate soil temperatures in winter. The physically-based soil temperature approach better matched observations due to its capability of better accounting for snow insulation effects.

We further analyzed simulated vs. observed total frozen days at the surface and different soil depths by TSWAT as shown in Fig. 6. Similar to the results derived from soil temperature simulation as discussed in Section 3.2, it is not surprising to find that TSWAT performed better for capturing frozen days for top soil layers than for deep layers. For example, for the four northern stations, P_{bias} ranged from −7 to 8%, from −17 to 32%, from −22 to 45%, from −16 to 37%, and from −49 to 360% at the surface and 5, 10, 20, and 50 cm depths, respectively. Note that, for the two southern stations, TSWAT generally performed poorer than the four northern stations, particularly for the station MO23909.

Table 5
Model performance on monthly stream flow by two versions of SWAT model in the UMRB for different periods.

Period	SWAT			TSWAT		
	R^2	NS	P_{bias} (%)	R^2	NS	P_{bias} (%)
Annual	0.71	0.54	21	0.81	0.68	18
Winter	0.67	0.45	14	0.86	0.70	16
Non-Winter	0.76	0.67	22	0.79	0.74	14

The reason for the relatively poor performance at the southern stations may be due to the rapid snow cover appearance and disappearance in the southern climate which is difficult to accurately simulated by TSWAT. The accuracy of the physically-based soil temperature is largely depended on surface conditions such as snow cover dynamics. In the northern climate, the snow cover develops gradually over winter, while in the south surface conditions are rather unstable which causes difficulty in simulation of soil frozen status.

3.4. Model performance evaluation for frozen depth

We also evaluated TSWAT-simulated freeze-thaw cycles based on observations of soil profile temperature and frozen depth. Fig. 7 compares the simulated vertical soil temperature profile by TSWAT with the observations at the six USCRN stations. The frozen depth in the simulated and observed soil profile is indicated by light bluish colors (temperature ≤ 0 °C) for different stations. The model reproduced the daily variations in frozen depth well, except that the depth was underestimated at WI54903 by approximately 20 cm and overestimated at IL54811 and two southern stations by approximately 20–40 cm. In general, the TSWAT model simulations captured well the seasonal changes of frozen depths in the soil profile across the six stations (Fig. 7).

3.5. Sensitivity of hydrological modeling to freeze-thaw cycle representation

We applied TSWAT to simulate monthly stream flow at USGS gauge station # 05587450 (Fig. 1) from 1980 to 2015. Meanwhile, the original SWAT model was used for comparison. Note that neither version of the SWAT model was calibrated for hydrology. The only difference between these two versions of the SWAT model is that one used the empirical soil temperature and another one used the calibrated new soil temperature module. Model performance evaluation results on monthly stream flow are summarized for annual, winter (Nov. to Apr.), and non-winter seasons are shown in Table 5. Time series of observed and simulated monthly stream flow by the two versions of SWAT model at

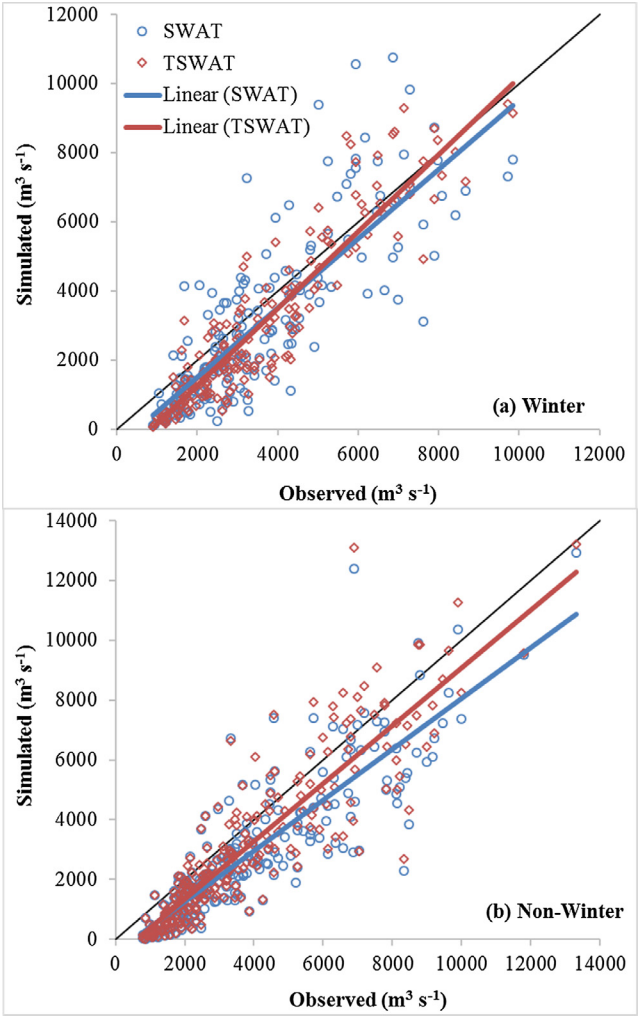

Fig. 9. Observed vs. simulated monthly stream flow at USGS gauge station # 05587450 for the two versions of SWAT model in (a) winter and (b) non-winter seasons from 1980 to 2015.

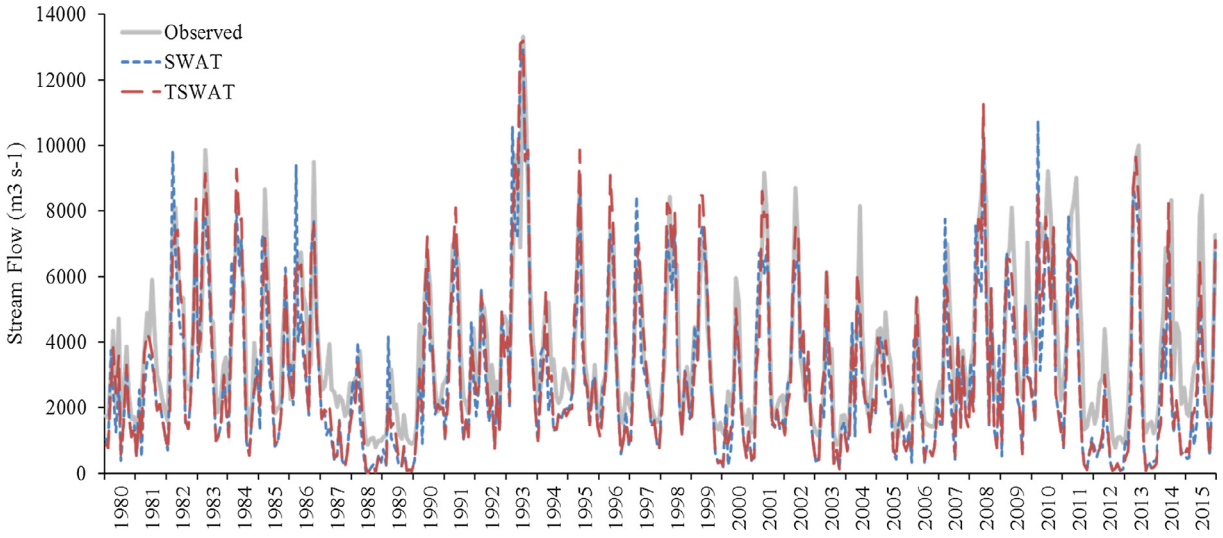

Fig. 8. Observed and simulated monthly stream flow at USGS gauge station # 05587450 for the two versions of SWAT model from 1980 to 2015.

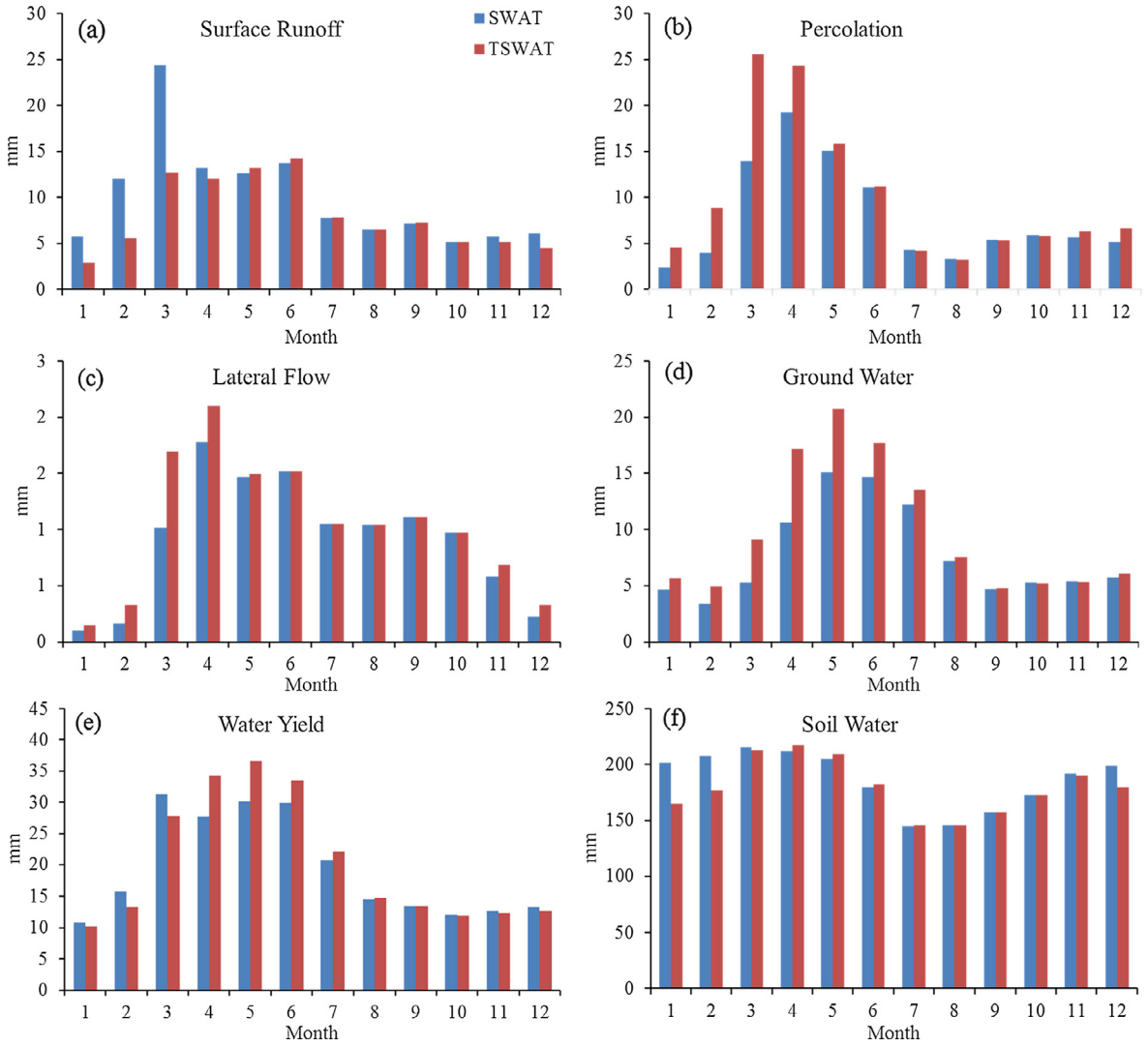

Fig. 10. Simulated average monthly surface runoff, percolation, lateral flow, ground water discharge, total water yield, and soil water (mm) from 1980 to 2015 in the UMRB by TSWAT and SWAT.

Table 6
Average annual surface runoff, percolation, lateral flow, ground water discharge, total water yield, and soil water (mm) from 1980 to 2015 in the UMRB simulated by TSWAT and SWAT and the percent difference values.

	Surface runoff (mm)	Lateral flow (mm)	Percolation (mm)	Ground water (mm)	Water yield (mm)	Soil water (mm)
SWAT	120	11	95	94	233	186
TSWAT	97	13	122	118	243	179
Percent difference (%)	−19	13	28	25	5	−4

USGS gauge station # 05587450 are shown in Fig. 8. Scatter plots of observed vs. simulated monthly stream flow at the station for the two versions of SWAT model in winter and non-winter are shown in Fig. 9.

All values of R^2 and NS generated with TSWAT were greater than the corresponding values generated with the original SWAT model and most absolute values of P_{bias} of TSWAT were less than those of the original SWAT model except for that in winter (Table 5). In general, the variation of simulated stream flow was consistent with the observed for the two versions of SWAT model (Fig. 8). Regression slope achieved by TSWAT was closer to the 1:1 line in winter and non-winter periods than the original SWAT model, and simulations by TSWAT had a stronger association with observations than those by the original SWAT, especially during winter (Fig. 9a and b). As shown in Table 5, TSWAT greatly improved stream flow simulation in winter (R^2 increased by 0.19 and NS by 0.15) compared with the original SWAT model. For non-winter seasons, TSWAT also slightly improved R^2 by 0.03 and NS by 0.07. We found that TSWAT exhibited slightly damped snowmelt flow peaks compared with the original SWAT model, which is the major reason for improved model performance in winter. TSWAT tended to generate more infiltration and less surface runoff during winter and snowmelt season on the watershed scale. The new soil temperature module better accounted for snowpack insulation effects on soil temperature allowing surface soil layers to remain unfrozen when snow accumulating on the ground. Collectively, the enhanced SWAT model improved its simulation of hydrological effects of freeze-thaw cycles, particularly during winter and the snowmelt season.

To illustrate the impacts of different freeze-thaw cycle representation on hydrology, we compared simulated monthly average surface

runoff, percolation, lateral flow, ground water discharge, total water yield, and soil moisture in the UMRB from 1980 to 2015 as shown in Fig. 10. Table 6 provides annual average statistical comparison by the two versions of SWAT model. In Table 6, the relative difference between results of both models is evaluated by percent difference (%), i.e., (simulated by TSWAT − simulation by SWAT)/simulation by SWAT × 100. Compared with SWAT, TSWAT generated much more percolation, lateral flow, and ground water discharge (percent difference = 28, 13, and 25%, respectively), less surface runoff and soil moisture (percent difference = −19 and −4%) on the annual scale. Total water yield was also increased by 5% based on the evaluation period of 1980 to 2015 (Table 6). Fig. 10 evidently explained the differences between simulations of SWAT and TSWAT on the monthly scale. Because soil frozen days and depths simulated by TSWAT were less than those of SWAT, more infiltration was generated and that water was easily transported downwards from soil profile eventually becoming recharge (percolation from soil profile) to aquafers and lateral flow during winter and the snowmelt season (Fig. 10b and c). TSWAT-generated ground water during winter slowly discharged to streams as base flow until summer months leading to prolonged differences between monthly ground water discharges of TSWAT and SWAT (see the comparison from Jan. to Jul. in Fig. 10d). Apparently, the corresponding surface runoff simulated by TSWAT was less than those of SWAT during winter months (noticing that the dramatic difference in surface runoff in March; Fig. 10a). Interestingly, SWAT produced more total water yield than TSWAT from Dec. to Mar. (next year) while TSWAT had more total water yield from Apr. to Jul. (Fig. 10e), which can be explained by the differences between TSWAT and SWAT in terms of surface runoff and ground water discharge in Fig. 10a and d. The original SWAT model tended to retain a large amount of frozen water in soils before soil thawing and resulted in overestimated soil water during winter months, while TSWAT reduced soil water content during this period leading to slight reduction in soil moisture (Fig. 10f) as indicated in Table 6 on the annual scale (percent difference = −4% which is close to the increase of total water yield of 5%).

4. Conclusion

In this study, we present the comparison between a physically-based soil temperature module and an empirical soil temperature module for simulating freeze-thaw cycles in the Upper Mississippi River Basin. Daily surface and soil temperature records at 5, 10, 20, 50, and 100 cm depths derived from six stations of the U.S. Climate Reference Network in the UMRB were used to evaluate model performance. Further, long-term streamflow data was used to understand the implications of improvements in freeze-thaw cycle representation for hydrological modeling using the modified version of SWAT (equipped with the physically-based soil temperature model, i.e., TSWAT) and the original version of SWAT (equipped with the original empirical soil temperature model). Detailed analyses and statistical assessment demonstrate that compared with the original SWAT model, TSWAT can reliably simulate surface and soil temperatures and frozen depth and days at six sites across the UMRB. The differences in freeze-thaw cycle representation between SWAT and TSWAT translate into noticeable discrepancies in simulated key hydrologic variables, such as surface runoff, lateral flow, percolation, and ground water discharge. Compared against long-term observed streamflow (1980–2015), TSWAT outperforms SWAT in capturing variations in monthly streamflow in both winter and non-winter seasons. These results and analyses demonstrate the importance of improving freeze-thaw cycle representation for enhanced hydrologic modeling in watersheds like the UMRB that are subject to freeze-thaw cycles.

Declaration of interests

The authors declared that there is no conflict of interest.

Acknowledgement

The funding support for this project was provided by NASA (NNX17AE66G and NNH13ZDA001N), and USDA (2017-67003-26485), and NSF INFEWS (1639327).

References

Arnold, J.G., Muttiah, R.S., Srinivasan, R., Allen, P.M., 2000. Regional estimation of base flow and groundwater recharge in the Upper Mississippi river basin. J. Hydrol. 227 (1–4), 21–40.
Arnold, J.G., Srinivasan, R., Muttiah, R.S., Williams, J.R., 1998. Large area hydrologic modeling and assessment part I: Model development. JAWRA J. Am. Water Resour. Assoc. 34 (1), 73–89.
Bélanger, J.A., 2009. Modelling soil temperature on the boreal plain with an emphasis on the rapid cooling period. Master Thesis Thesis, Lakehead University.
Cary, J., 1966. Soil moisture transport due to thermal gradients: practical aspects 1. Soil Sci. Soc. Am. J. 30 (4), 428–433.
Cheng, Q., et al., 2014. In situ measured and simulated seasonal freeze–thaw cycle: a 2-year comparative study between layered and homogeneous field soil profiles. J. Hydrol. 519, 1466–1473.
Cherkauer, K.A., Lettenmaier, D.P., 1999. Hydrologic effects of frozen soils in the upper Mississippi River basin. J. Geophys. Res.: Atmos. 104 (D16), 19599–19610.
Fontaine, T., Cruickshank, T., Arnold, J., Hotchkiss, R., 2002. Development of a snowfall–snowmelt routine for mountainous terrain for the soil water assessment tool (SWAT). J. Hydrol. 262 (1), 209–223.
Gassman, P.W., Reyes, M.R., Green, C.H., Arnold, J.G., 2007. The soil and water assessment tool: historical development, applications, and future research directions. Trans. ASABE 50 (4), 1211–1250.
Groffman, P.M., et al., 2001. Colder soils in a warmer world: a snow manipulation study in a northern hardwood forest ecosystem. Biogeochemistry 56 (2), 135–150.
Harlan, R., 1973. Analysis of coupled heat-fluid transport in partially frozen soil. Water Resour. Res. 9 (5), 1314–1323.
Hayashi, M., van der Kamp, G., Schmidt, R., 2003. Focused infiltration of snowmelt water in partially frozen soil under small depressions. J. Hydrol. 270 (3–4), 214–229.
Hillel, D., 1980. Fundamentals of Soil Physics. Academic Press, Inc. (London) Ltd.
Iwata, Y., et al., 2011. Influence of rain, air temperature, and snow cover on subsequent spring-snowmelt infiltration into thin frozen soil layer in northern Japan. J. Hydrol. 401 (3–4), 165–176.
Jha, M., Gassman, P.W., Secchi, S., Gu, R., Arnold, J., 2004. Effect of watershed subdivision on swat flow, sediment, and nutrient predictions. JAWRA J. Am. Water Resour. Assoc. 40 (3), 811–825.
Johansen, O., 1975. Thermal conductivity of soils. Ph.D. Thesis, Trondheim, Norway (CRREL Draft Translation 637, 1977) ADA 044002.
Jonas, T., Marty, C., Magnusson, J., 2009. Estimating the snow water equivalent from snow depth measurements in the Swiss Alps. J. Hydrol. 378 (1), 161–167.
Li, Q., et al., 2014. An approach for assessing impact of land use and biophysical conditions across landscape on recharge rate and nitrogen loading of groundwater. Agric. Ecosyst. Environ. 196, 114–124. https://doi.org/10.1016/j.agee.2014.06.028.
Li, Z., Fang, H., 2016. Impacts of climate change on water erosion: a review. Earth Sci. Rev. 163, 94–117.
Luo, L., et al., 2003. Effects of frozen soil on soil temperature, spring infiltration, and runoff: results from the PILPS 2 (d) experiment at Valdai, Russia. J. Hydrometeorol. 4 (2), 334–351.
Meng, F.R., Bourque, C.A., Jewett, K., Daugharty, D., Arp, P.A., 1995. The Nashwaak experimental watershed project: analysing effects of clearcutting on soil temperature, soil moisture, snowpack, snowmelt and stream flow. Water Air Soil Pollut. 82 (1–2), 363–374.
Mitchell, K.E., et al., 2004. The multi-institution North American Land Data Assimilation System (NLDAS): utilizing multiple GCIP products and partners in a continental distributed hydrological modeling system. J. Geophys. Res.: Atmos. 109 (D7).
Moriasi, D.N., et al., 2007. Model evaluation guidelines for systematic quantification of accuracy in watershed simulations. Trans. ASABE 50 (3), 885–900.
Neitsch, S.L., Williams, J.R., Arnold, J.G., Kiniry, J.R., 2011. Soil and Water Assessment Tool Theoretical Documentation Version 2009. Grassland Soil and Water Research Service Temple, Texas, USA.
Ouyang, W., Liu, B., Wu, Y., 2016. Satellite-based estimation of watershed groundwater storage dynamics in a freeze–thaw area under intensive agricultural development. J. Hydrol. 537, 96–105.
Qi, J., Li, S., Bourque, C.P., Xing, Z., Fan-Rui, M., 2018a. Developing a decision support tool for assessing land use change and BMPs in ungauged watersheds based on decision rules provided by SWAT simulation. Hydrol. Earth Syst. Sci. 22 (7), 3789–3806.
Qi, J., et al., 2017. Modifying SWAT with an energy balance module to simulate snowmelt for maritime regions. Environ. Modell. Software 93, 146–160.
Qi, J., et al., 2016a. Assessing an enhanced version of SWAT on water quantity and quality simulation in regions with seasonal snow cover. Water Resour. Manage. 30 (14), 5021–5037.
Qi, J., et al., 2016b. A new soil-temperature module for SWAT application in regions with seasonal snow cover. J. Hydrol. 538, 863–877.
Qi, J., et al., 2018b. Assessing the performance of a physically-based soil moisture module integrated within the Soil and Water Assessment Tool. Environ. Modell. Software 109, 329–341.

Riseborough, D., 1990. Soil latent heat as a filter of the climate signal in permafrost. Proceedings of the Fifth Canadian Permafrost Conference, Collect. Nordicana. Citeseer, pp. 199–205.
Shanley, J.B., Chalmers, A., 1999. The effect of frozen soil on snowmelt runoff at Sleepers River, Vermont. Hydrol. Process. 13 (12–13), 1843–1857.
Slater, A., Pitman, A., Desborough, C., 1998. Simulation of freeze-thaw cycles in a general circulation model land surface scheme. J. Geophys. Res.: Atmos. 103 (D10), 11303–11312.
Solomon, S., 2007. Climate Change 2007-The Physical Science Basis: Working Group I Contribution to the Fourth Assessment Report of the IPCC, 4. Cambridge University Press.
Srinivasan, R., Zhang, X., Arnold, J., 2010. SWAT ungauged: hydrological budget and crop yield predictions in the Upper Mississippi River Basin. Trans. ASABE 53 (5), 1533–1546.
Steppuhn, H., 1981. Snow and agriculture. Handbook of snow, principles, processes, management and use. Pergamon, Toronto, pp. 60–126.
Sturm, M., Holmgren, J., König, M., Morris, K., 1997. The thermal conductivity of seasonal snow. J. Glaciol. 43 (143), 26–41.
Verseghy, D.L., 1991. CLASS—a Canadian land surface scheme for GCMs. I. Soil model. Int. J. Climatol. 11 (2), 111–133.
Wang, G., Hu, H., Li, T., 2009. The influence of freeze–thaw cycles of active soil layer on surface runoff in a permafrost watershed. J. Hydrol. 375 (3–4), 438–449.
Wellen, C., Kamran-Disfani, A.-R., Arhonditsis, G.B., 2015. Evaluation of the current state of distributed watershed nutrient water quality modeling. Environ. Sci. Technol. 49 (6), 3278–3290.
Williams, P.J., Smith, M.W., 1991. The frozen earth.
Woo, M.K., Arain, M., Mollinga, M., Yi, S., 2004. A two-directional freeze and thaw algorithm for hydrologic and land surface modelling. Geophys. Res. Lett. 31 (12).
Wu, J., Tanaka, K., 2005. Reducing nitrogen runoff from the upper Mississippi River basin to control hypoxia in the Gulf of Mexico: easements or taxes? Mar. Resour. Econ. 20 (2), 121–144.
Xia, Y., et al., 2012. Continental-scale water and energy flux analysis and validation for the North American Land Data Assimilation System project phase 2 (NLDAS-2): 1. Intercomparison and application of model products. J. Geophys. Res.: Atmos., 117(D3).
Yin, X., Arp, P.A., 1993. Predicting forest soil temperatures from monthly air temperature and precipitation records. Can. J. For. Res. 23 (12), 2521–2536.
Yuan, Y., Locke, M.A., Bingner, R.L., Rebich, R.A., 2013. Phosphorus losses from agricultural watersheds in the Mississippi Delta. J. Environ. Manage. 115, 14–20.
Zhang, C., Li, S., Qi, J., Xing, Z., Meng, F., 2017. Assessing impacts of riparian buffer zones on sediment and nutrient loadings into streams at watershed scale using an integrated REMM-SWAT model. Hydrol. Process. 31 (4), 916–924.
Zhang, T., 2005. Influence of the seasonal snow cover on the ground thermal regime: an overview. Rev. Geophys. 43 (4).
Zhao, L., Gray, D.M., Male, D.H., 1997. Numerical analysis of simultaneous heat and mass transfer during infiltration into frozen ground. J. Hydrol. 200 (1–4), 345–363.
Zheng, D., et al., 2018. Impact of soil freeze-thaw mechanism on the runoff dynamics of two Tibetan rivers. J. Hydrol. 563, 382–394.